Spatio-temporal variation in the composition of the solar spectrum and its possible evolution

Irina Kolomiets

Institute of Ecology and Geography, Academy of Sciences of Republic of Moldova, Chişinău, Republic of Moldova. Corresponding author: I. Kolomiets, kolomiec71@gmail.com

Abstract. This paper presents data on the variation of qualitative characteristics (spectral composition, position of the maximum and short-wavelength boundary) of the solar spectrum in the ultraviolet and visible regions. The latitudinal and seasonal distribution of solar radiation maximum has been established. It is hypothesized that the corolla color of flowering plants is the result of adaptation to the solar spectrum maximum.
Kee Words: adaptation, corolla color, position of the maximum, solar irradiance, spectral composition.

Introduction. One of the most important factors of evolution are ecological changes caused by periodic fluctuations in solar activity, as pointed out by Chizhevsky (1976): “The reason for organic evolution lies in disturbances in the physical state and chemical composition of the external environment under the influence of sharp fluctuations or disturbances in nature associated with fluctuations in solar activity". All the most diverse and varied phenomena on Earth, including the variety of organic life, are caused by variation of energy flows that burst into the atmosphere in the form of solar radiation. Light, as one of the most important environmental factors, in addition to providing energy, also performs a regulatory function in a plant. It acts as an inductor of the main mechanisms of endogenous regulation. In the widely used ecocenotic scales of Landolt (1977), Tsyganov (1983), and Ellenberg (1996), plants are classified on the basis of the quantitative characteristic of solar energy - total solar radiation. Despite the huge amount of data on the selective effect of some regions of solar radiation on all living things and on plants in particular, there is no single classification that takes into account the adaptation of plants both separately to the qualitative characteristics of solar radiation, and together with quantitative ones. The purpose of this work was to study the details of distribution of qualitative characteristics of solar radiation (spectral composition, position of the maximum and short-wavelength boundary).

Material and Method. The study was carried out in 2019-2021. The analysis of the qualitative characteristics of solar radiation was based on data from NASA Technical Memorandum 82021 (Mecherikunnel & Richmond 1980) for absolutely clear sky ($\alpha = 1.3$, $\beta = 0.02$) at water vapor pressure $H_2O = 20$ mm and ozone pressure $O_3 = 3.4$ mm. For the mean wavelength of the color regions the flux energy were calculated in $W/m^2 \cdot nm$. For the calendar dates of solstice and equinox the air masses at different Sun heights were calculated by the Bemporad table (Ismagilov 2019). The flowering start time and corolla color of the potential flora of the Balti steppe was determined according to the Ciocârlan (2000) guide.

Results and Discussion. The main qualitative characteristics of solar radiation are spectral composition, position of maximum and position of the short-wavelength boundary, which depend on the height of the Sun above the horizon and on the optical mass of the atmosphere (Table 1). The lower the sun goes down, the richer its spectrum is in long-wave (red-orange) radiation, and the short-wavelength boundary and maximum radiation are shifted towards longer wavelengths. Since the Sun does not rise above the horizon higher than 6.5-16.5º at latitudes 50-60° in winter months, it follows that in winter at these latitudes in the solar spectrum, ultraviolet radiation with wavelengths shorter than 360 nm is completely absent. In summer, the ultraviolet end of the spectrum extends up to 295 nm.

Table 1

Daylight means of the Sun's altitude above the horizon (h°) and atmospheric optical mass (m) at the dates of solstice and equinox at different latitudes

Date	*December 22*		*March 21*		*June 21*		*September 23*	
Latitude, °	*h*	*m*	*h*	*m*	*h*	*m*	*h*	*m*
90	-	-	0	39.600	23.5	2.500	0	39.600
80	-	-	10	10.400	33,5	2.500	10	10.400
70	-	-	20	5.600	43.5	2.500	20	5.600
60	6.5	14.650	30	3.820	53.5	2.220	30	3.820
50	16.5	6.720	40	2.900	63.5	1.895	40	2.900
40	26.5	4.300	50	2.360	73.5	1.670	50	2.360
30	36.5	3.170	60	2.000	83.5	1.500	60	2.000
20	46.5	2.525	70	1.740	86.5	1.455	70	1.740
10	56.5	2.105	80	1.550	76.5	1.610	80	1.550
0	66.5	1.820	90	1.410	66.5	1.820	90	1.410
-10	76.5	1.610	80	1.550	56.5	2.105	80	1.550
-20	86.5	1.455	70	1.740	46.5	2.525	70	1.740
-30	83.5	1.500	60	2.000	36.5	3.170	60	2.000
-40	73.5	1.670	50	2.360	26.5	4.300	50	2.360
-50	63.5	1.895	40	2.900	16.5	6.720	40	2.900
-60	53.5	2.220	30	3.820	6.5	14.650	30	3.820
-70	43.5	2.500	20	5.600	-	-	20	5.600
-80	33.5	2.500	10	10.400	-	-	10	10.400
-90	23.5	2.500	0	39.600	-	-	0	39.600

Notes:
1. the gray color gradient indicates the decrease in optical mass;
2. "-" = polar night;
3. the "-" sign in the first column denotes the latitude of the southern hemisphere.

At the moments of the vernal and autumnal equinox, the height of the Sun above the horizon (h,°) and optical mass (m) change symmetrically relative to the equator line (0°) - decrease in the direction from the North pole to the equator and increase from the equator to the South pole. At the time of the winter solstice, the center of symmetry shifts to the South pole by 23°, causing the phenomenon of polar night at the North pole and the phenomenon of polar day at the South pole. At the moment of the summer solstice, the center of symmetry shifts to the North pole by 23°, causing the phenomenon of polar night at the South pole and the phenomenon of polar day at the North pole. It is easy to see that the variation of the Sun's altitude above the horizon and optical mass is sinusoidal and causes a change in the main qualitative characteristics of solar radiation: spectral composition, position of maximum and short-wavelength boundary (Table 2).

Latitudinal analysis of the distribution of solar energy maxima by regions of the visible spectrum showed that in the interval between 30° North latitude and 30° South latitude at the dates of the spring and autumn equinox (Table 2), solar energy maxima lie in the blue region (495 nm) of the visible spectrum, with the absolute values of the maxima increase from the poles to the equator. At the 40th latitudes, the maximum shifts to the green region (530 nm). In the yellow (580 nm) and orange (610 nm) regions, no maxima were found in the indicated dates, and starting from the 50th latitudes, the energy maximum shifts to the red region (660-680 nm), and in the far red region (730 nm) the energy decreases at all latitudes in the annual cycle.

At the time of the winter solstice, the absorption maximum in the blue region (495 nm) begins at 10° North latitude and continues to 60° Ssouth latitude. In the zone of 20° North latitude and in the zone from 70 to 90° South latitude (polar zone), two extremum points are observed, in the green and red regions. From 30° to 60° Northern latitude, the maxima are localized in the *near* (660 nm) and *middle* (680 nm) red regions. The division of the red region into *near, middle* and *far* (730 nm) is caused by the need to distinguish the far red zone as an energy minimum zone (even in comparison with the near infrared). In addition, the choice of these intervals is motivated by absorption spectra of phytochrome (λ = 660 nm in the red and λ = 730 nm in the far red), a trigger of plant morphogenesis. In particular, phytochrome plays an important role in a number of processes, such as flowering and seed germination (Golovatskaya 2005).

At the time of the summer solstice, the maximum in the blue region begins at 60°N and continues to 10°S. In the northern polar region (70°-90°N) and at 20°S, the maximum shifts to the green region of the spectrum (530 nm). At the same latitudes, a second maximum appears in the near red (660 nm), which in the southern hemisphere is replaced by a peak in the middle red, in the belt 40°-60°S.

Expression of the qualitative characteristics of solar radiation is, therefore, cyclical and can cause a similar response in biological systems, manifested in the form of adaptations both at the zonal (latitudinal) and seasonal levels. Biological adaptation could follow the path of the formation of light-sensitive surfaces in living organisms, the absorption maximum of which coincides with the spectral maximum of the incident radiation. For such surfaces, the general laws of absorption of electromagnetic radiation are satisfied. They determine the relationship between the amount of absorption and the amount of absorbing substance (pigment). Pigments are characterized by a specific molecular structure, namely, the presence of a system of conjugated double bonds. Depending on the position and number of double bonds, the pigment absorbs the light of some parts of the visible (white) spectrum, with a certain wavelength. Therefore, each pigment has a corresponding color and a specific light absorption curve. The more double bonds in the pigment molecule, the longer its absorption wave. According to the Grotthuss-Draper law (Protti & Fagnoni 2009), the chemical transformation of a substance can only be caused by the light absorbed by this substance, or in other words, only such light chemically acts on a colored body, the color of which is complementary to the body color, that is, which complements body color to white (Figure 1, Table 3).

Table 2

Solar energy flux (E, W/m^2·nm) at the different points of the visible spectrum (λ, nm) at different latitudes on the days of the winter (December 22) and summer (June 21) solstices and the spring and autumn equinox (March 21, September 23)

Latitude, β°	*Daylight mean optical mass*	*λ, nm (December 22)*										
		315	*360*	*410*	*465*	*495*	*530*	*580*	*610*	*660*	*680*	*730*
90	-	-	-	-	-	-	-	-	-	-	-	-
80	-	-	-	-	-	-	-	-	-	-	-	-
70	-	-	-	-	-	-	-	-	-	-	-	-
60	14.650	0.00	0. 126	6.406	49.60	117.02	120.38	159.95	203.89	350.90	395.14	221.73
50	6.720	0.00	15.18	135.74	219.46	478.4	531.38	585.70	640.37	761.24	785.16	517.55
40	4.300	0.10	70.76	344.19	679.08	792.37	832.00	862.77	885.14	968.45	974.57	670.94
30	3.170	0.85	143.49	528.69	907.55	999.19	1024.54	1032.33	1038.89	1082.25	1079.17	763.19
20	2.525	5.23	222.27	682.61	1074.66	1148.62	1156.05	1145.95	1140.08	1154.52	1142.47	826.70
10	2.105	9.01	212.19	793.07	1191.42	1252.00	1246.35	1223.65	1208.96	1203.24	1184.89	869.80
0	1.820	23.88	218.00	891.37	1286.84	1333.72	1316.73	1283.00	1261.11	1239.04	1215.84	903.90
-10	1.610	40.07	400.70	972.31	1362.48	1397.56	1371.24	1328.44	1300.91	1255.92	1238.98	931.79
-20	1.455	51.63	440.59	1030.12	1416.51	1443.16	1410.18	1360.91	1329.33	1285.12	1255.51	951.71
-30	1.500	48.55	429.95	1014.70	1402.10	1431.00	1399.80	1352.25	1321.75	1273.60	1251.10	946.40
-40	1.670	35.44	384.75	949.182	1340.87	1379.32	1355.67	1315.45	1289.54	1258.54	1232.97	923.82
-50	1.895	17.17	323.60	860.54	1258.02	1309.4	1295.96	1265.65	1245.95	1228.80	1207.02	893.94
-60	2.220	8.02	265.98	764.14	1160.84	1224.88	1222.70	1203.30	1190.92	1111.60	1173.78	857.45
-70	2.500	5.50	226.50	690.00	1083.00	1156.00	1162.50	1151.00	1145.00	1158.00	1245.50	828.75
-80	2.500	5.50	226.50	690.00	1083.00	1156.00	1162.50	1151.00	1145.00	1158.00	1245.50	828.75
-90	2.500	5.50	226.50	690.00	1083.00	1156.00	1162.50	1151.00	1145.00	1158.00	1245.50	828.75

		λ, nm (March 21, September 23)										
Latitude, β°	*Daylight mean optical mass*	*315*	*360*	*410*	*465*	*495*	*530*	*580*	*610*	*660*	*680*	*730*
		0	0	0	0.09	0.58	1.28	3.17	6.24	32.54	46.02	7.14
80	10.40	0	0.48	32.96	141.62	226.26	267.28	323.20	369.28	526.14	569.92	358.92
70	5.60	0	31.30	209.32	243.50	625.52	656.84	703.80	738.36	855.73	769.88	578.92
60	3.82	0.26	95.65	412.79	768.19	869.90	908.06	930.34	946.56	1014.39	1018.66	708.13
50	2.90	0.19	170.1	585.30	971.80	1057.60	1076.50	1077.50	1079.40	1111.60	1105.10	787.75
40	2.36	0.68	246.24	727.32	1121.92	1190.44	1192.60	1177.40	1167.96	1174.24	1159.64	843.10
30	2.00	10.00	297.0	822.00	1222.00	1279.00	1270.00	1244.00	1227.00	1216.00	1196.00	880.00
20	1.74	30.05	366.13	922.20	1315.65	1358.04	1337.50	1299.79	1276.27	1249.28	1224.65	914.53
10	1.55	44.70	416.66	995.43	1384.10	1415.80	1386.82	1341.43	1514.83	1273.60	1245.60	939.76
0	1.41	55.49	453.88	1049.39	1434.52	1458.36	1423.64	1371.24	1338.81	1291.52	1261.02	958.35
-10	1.55	44.70	416.66	995.43	1384.10	1415.80	1386.82	1341.43	1514.83	1273.60	1245.60	939.76
-20	1.74	30.05	366.13	922.20	1315.65	1358.04	1337.50	1299.79	1276.27	1249.28	1224.65	914.53
-30	2.00	10.00	297.0	822.00	1222.00	1279.00	1270.00	1244.00	1227.00	1216.00	1196.00	880.00
-40	2.36	0.68	246.24	727.32	1121.92	1190.44	1192.60	1177.40	1167.96	1174.24	1159.64	843.10
-50	2.90	0.19	170.1	585.30	971.80	1057.60	1076.50	1077.50	1079.40	1111.60	1105.10	787.75
-60	3.82	0.26	95.65	412.79	768.19	869.90	908.06	930.34	946.56	1014.39	1018.66	708.13
-70	5.60	0	31.30	209.32	243.50	625.52	656.84	703.80	738.36	855.73	769.88	578.92
-80	10.40	0	0.48	32.96	141.62	226.26	267.28	323.20	369.28	526.14	569.92	358.92
-90	39.60	0	0	0	0.09	0.58	1.28	3.17	6.24	32.54	46.02	7.14

		λ, nm (June 21)										
Latitude, β°	*Daylight mean optical mass*	*315*	*360*	*410*	*465*	*495*	*530*	*580*	*610*	*660*	*680*	*730*
90	2.50	5.50	226.50	690.00	1083.00	1156.00	1162.50	1151.00	1145.00	1158.00	1245.50	828.75
80	2.50	5.50	226.50	690.00	1083.00	1156.00	1162.50	1151.00	1145.00	1158.00	1245.50	828.75
70	2.50	5.50	226.50	690.00	1083.00	1156.00	1162.50	1151.00	1145.00	1158.00	1245.50	828.75
60	2.22	8.02	265.98	764.14	764.14	1224.88	1222.70	1203.30	1190.92	1190.00	1173.78	857.45
50	1.89	17.17	323.60	860.54	860.54	1309.4	1295.96	1265.65	1245.95	1228.80	1207.02	893.94
40	1.67	35.44	384.75	949.182	949.182	1379.32	1355.67	1315.45	1289.54	1258.54	1232.97	923.82
30	1.50	48.55	429.95	1014.70	1014.70	1431.00	1399.80	1352.25	1321.75	1273.60	1251.10	946.40
20	1.45	51.63	440.59	1030.12	1030.12	1443.16	1410.18	1360.91	1329.33	1285.12	1255.51	951.71
10	1.61	40.07	400.70	972.31	972.31	1397.56	1371.24	1328.44	1300.91	1255.92	1238.98	931.79
0	1.82	23.88	218.00	891.37	891.37	1333.72	1316.73	1283.00	1261.11	1239.04	1215.84	903.90
-10	2.10	9.01	212.19	793.07	793.07	1252.00	1246.35	1223.65	1208.96	1203.24	1184.89	869.80
-20	2.52	5.23	222.27	682.61	682.61	1148.62	1156.05	1145.95	1140.08	1154.52	1142.47	826.70
-30	3.17	0.85	143.49	528.69	528.69	999.19	1024.54	1032.33	1038.89	1082.25	1079.17	763.19
-40	4.30	0.1	70.76	344.19	344.19	792.37	832.00	862.77	885.14	968.45	974.57	670.94
-50	6.72	0	15.18	135.74	135.74	478.4	531.38	585.70	640.37	761.24	785.16	517.55
-60	14.65	0	0. 126	6.406	6.406	117.02	120.38	159.95	203.89	350.90	395.14	221.73
-70	-	-	-	-	-	-	-	-	-	-	-	-
-80	-	-	-	-	-	-	-	-	-	-	-	-
-90	-	-	-	-	-	-	-	-	-	-	-	-

Notes:
1. the gray color gradient indicates the decrease in optical mass;
2. "-" = polar night;
3. the "-" sign in the first column denotes the latitude of the southern hemisphere.

Table 3

Color palette in additive RGB

Color	*Formation of color*	
	Reflected (main)	*Absorbed (complementary)*
Black	Black = 0 + 0 + 0	Black = R_{max} + G_{max} + B_{max}
White	White = R_{max} + G_{max} + B_{max}	White = 0 + 0 + 0
Red	Red = R_{max} + 0 + 0	Red = 0 + G_{max} + B_{max}
Green	Green = 0 + G_{max} + 0	Green = R_{max} + 0 + B_{max}
Blue	Blue = 0 + 0 + B_{max}	Blue = R_{max} + G_{max} + 0
Cyan	Cyan = 0 + G_{max} + B_{max}	Cyan = R_{max} + 0 + 0
Magenta	Magenta = R_{max} + 0 + B_{max}	Magenta = 0 + G_{max} + 0
Yellow	Yellow = R_{max} + G_{max} + 0	Yellow = 0 + 0 + B_{max}

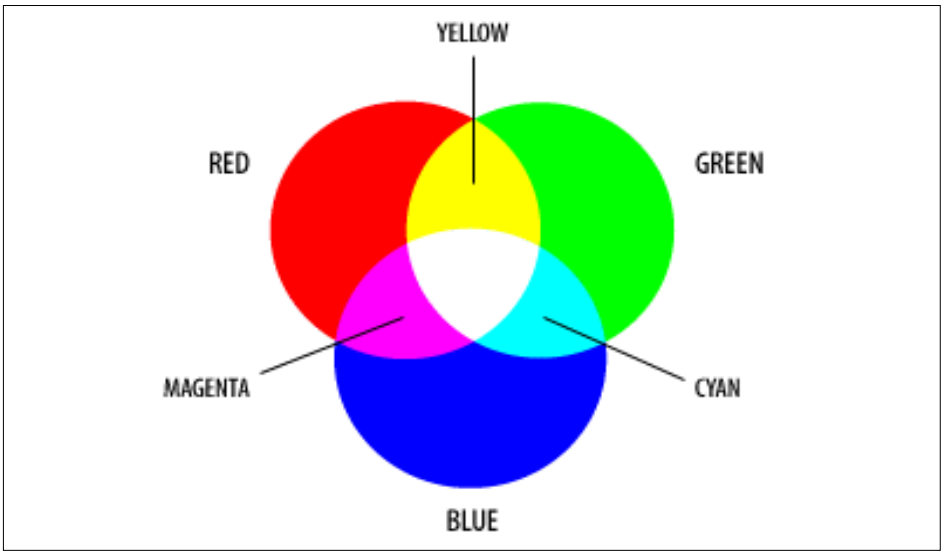

Figure 1. Color format RGB (webkyrs.info).

Using these formulas, we represent the color formation at surfaces that are optimally adapted to the maximum of solar radiation (Table 4).

Whence it follows that at the days of the spring and autumn equinox, the surface of yellow color will be optimally adapted to the blue maximum of radiation (from 30°S to 30°N). The zones 40°N and 40°S are characterized by the maximum irradiation in the green region, then according to the additive color rendering system RGB, the optimally adapted surface will be magenta, as a combination of red and blue. At the belt 50-90° in both the hemispheres, where the maximum radiation is in the red region, the best adapted surface will be blue-green cyan as a combination of green and blue. At the time of the winter solstice, the latitudinal maximums are shifted 23° South compared to the autumn equinox, and at the moment of the summer solstice, by 23° North compared to the vernal equinox. Accordingly, at the time of the summer solstice for the belt 10°S-60°N, the most adapted surface will be a yellow surface, and in the belt 20-90°S, the most adapted surface will be a blue-green (cyan) surface. Similar reasoning can be given for the day of the winter solstice. The presented material can serve as a rationale for the seasonal and zonal convergention of corolla color in flowering plants and a theoretical basis for creating an eco-coenotic scale based on the color of the corolla.

Table 4

Expected coloration of optimally adapted surfaces

Latitude	December 22		March 21		June 21		September 23	
	Max absorbed	*Max reflected*	*Max absorbed*	*Max reflected*	*Max absorbed*	*Max reflected*	*Max absorbed*	*Max reflected*
90°	-	-	R_{max}	$Cyan_{max}$	$R_{max}+G_{max}$	$Blue_{max}$	R_{max}	$Cyan_{max}$
80°	-	-	R_{max}	$Cyan_{max}$	$R_{max}+G_{max}$	$Blue_{max}$	R_{max}	$Cyan_{max}$
70°	-	-	R_{max}	$Cyan_{max}$	$R_{max}+G_{max}$	$Blue_{max}$	R_{max}	$Cyan_{max}$
60°	R_{max}	$Cyan_{max}$	R_{max}	$Cyan_{max}$	$Blue_{max}$	$Yellow_{max}$	R_{max}	$Cyan_{max}$
50°	R_{max}	$Cyan_{max}$	R_{max}	$Cyan_{max}$	$Blue_{max}$	$Yellow_{max}$	R_{max}	$Cyan_{max}$
40°	R_{max}	$Cyan_{max}$	G_{max}	Magenta	$Blue_{max}$	$Yellow_{max}$	G_{max}	Magenta
30°	R_{max}	$Cyan_{max}$	$Blue_{max}$	$Yellow_{max}$	$Blue_{max}$	$Yellow_{max}$	$Blue_{max}$	$Yellow_{max}$
20°	$R_{max}+G_{max}$	Magenta	$Blue_{max}$	$Yellow_{max}$	$Blue_{max}$	$Yellow_{max}$	$Blue_{max}$	$Yellow_{max}$
10°	$Blue_{max}$	$Yellow_{max}$	$Blue_{max}$	$Yellow_{max}$	$Blue_{max}$	$Yellow_{max}$	$Blue_{max}$	$Yellow_{max}$
0°	$Blue_{max}$	$Yellow_{max}$	$Blue_{max}$	$Yellow_{max}$	$Blue_{max}$	$Yellow_{max}$	$Blue_{max}$	$Yellow_{max}$
-10°	$Blue_{max}$	$Yellow_{max}$	$Blue_{max}$	$Yellow_{max}$	$Blue_{max}$	$Yellow_{max}$	$Blue_{max}$	$Yellow_{max}$
-20°	$Blue_{max}$	$Yellow_{max}$	$Blue_{max}$	$Yellow_{max}$	$R_{max}+G_{max}$	$Blue_{max}$	$Blue_{max}$	$Yellow_{max}$
-30°	$Blue_{max}$	$Yellow_{max}$	$Blue_{max}$	$Yellow_{max}$	R_{max}	$Cyan_{max}$	$Blue_{max}$	$Yellow_{max}$
-40°	$Blue_{max}$	$Yellow_{max}$	G_{max}	Magenta	R_{max}	$Cyan_{max}$	G_{max}	Magenta
-50°	$Blue_{max}$	$Yellow_{max}$	R_{max}	$Cyan_{max}$	R_{max}	$Cyan_{max}$	R_{max}	$Cyan_{max}$
-60°	$Blue_{max}$	$Yellow_{max}$	R_{max}	$Cyan_{max}$	R_{max}	$Cyan_{max}$	R_{max}	$Cyan_{max}$
-70°	$R_{max}+G_{max}$	Magenta	R_{max}	$Cyan_{max}$	-	-	R_{max}	$Cyan_{max}$
-80°	$R_{max}+G_{max}$	$Blue_{max}$	R_{max}	$Cyan_{max}$	-	-	R_{max}	$Cyan_{max}$
-90°	$R_{max}+G_{max}$	$Blue_{max}$	R_{max}	$Cyan_{max}$	-	-	R_{max}	$Cyan_{max}$

Notes:
1. "-" = polar night;
2. the "-" sign in the first column denotes the latitude of the southern hemisphere.

Conclusions. Summing up the above, we can conclude that:

- the expression of the qualitative characteristics of solar radiation is cyclical and causes a similar response in biological systems, manifested in the form of adaptations both at the zonal (latitudinal) and seasonal levels;
- on the dates of the spring and autumn equinox, the surface of yellow color will be maximally adapted to the blue-green maximum of radiation (from 30°S to 30°N). For latitudes of 40°S and 40°N, the purple surface will be the most adapted. Symmetrical peripheral latitudes from 50° to 90° with irradiation maximum in the red region form an optimally adapted blue-green (cyan) surface;
- on the days of the winter and summer solstices, a meridional shift of the radiation maxima by 23° is observed with a corresponding shift of the optimally adapted surfaces. At these dates, there are latitudes with two irradiation maxima, in the green and red regions of the spectrum. This combination of maxima forms an optimally adapted blue surface.

Acknowledgements. Research was carried out within the project of the State Program 20.8000.9.707.11 (2020-2023): “Evaluation of stability of urban and rural ecosystems in order to ensure their sustainable development", financed by the National Agency for Research and Development.

References

Chizhevsky A. L., 1976 [Earth echo of solar storms]. Ed. Misli, Moscow, 367 pp. [in Russian]

Ciocârlan V., 2000 Flora ilustrată a României. Ed. Cereş, Bucureşti, 1138 pp. [in Romanian]

Ellenberg H., 1996 Vegetation Mitteleuropas mit den Alpen in okologischer, dynamischer und historischer Sicht. Ed. Aufl. Ulmer, Stuttgart, 1096 pp. [in German]

Golovatskaya I. F., 2005 The role of cryptochrome 1 and phytochromes in the control of plant photomorphogenetic responses to green light. Russian Journal of Plant Physiology 52(6):724-730.

Ismagilov N. V., 2019 [Methodological instructions for practical training in the course Meteorology and Climatology]. Ed. KFU, Kazani, 71 pp. [in Russian]

Landolt E., 1977 Okologische Zeigerwerts zur Sweizer Flora. Veroff Geobot Inst ETH. Zurich, H. 64, pp. 1-208. [in German]

Mecherikunnel A. T., Richmond J., 1980 Spectral distribution of solar radiaton. Technical Memorandum 82021. zSAx Ed. NASA Greenbelt, Maryland, 93 pp.

Protti S., Fagnoni M., 2009 The sunny side of chemistry: green synthesis by solar light. Photochemical and Photobiological Sciences 8(11):1499-1516.

Tsyganov D. N., 1983 [Phytoindication of ecological regimes in the subzone of coniferous-broad-leaved forests]. Ed. Nauka, Moscow, 196 pp. [in Russian]

Received: 27 April 2021. Accepted: 22 May 2021. Published online: 12 June 2021.
Author:
Irina Kolomiets, Institute of Ecology and Geography, Academy of Sciences of Republic of Moldova, Chişinău, Republic of Moldova, e-mail: kolomiec71@gmail.com

How to cite this article:
Kolomiets I., 2021 Spatio-temporal variation in the composition of the solar spectrum and its possible evolution. Ecoterra 18(2):1-9.